DOI: 10.1002/ejic.200900119

Synthesis, Structure and Spectral, and Electrochemical Properties of New Mononuclear Ruthenium(III) Complexes of Tris[(benzimidazol-2-yl)-methyl]amine: Role of Steric Hindrance in Tuning the Catalytic Oxidation Activity

Mariappan Murali,[a] Ramasamy Mayilmurugan,[a] and Mallayan Palaniandavar*[a]

Keywords: Ruthenium(III) complexes / Electronic structure / Redox chemistry / Oxidation / Alkanes / Epoxidation / Alkenes / Ligand effects

The new mononuclear Ru^{III} complexes $[Ru(ntb)Cl_2]Cl$ (**1**), $[Ru(ntb)Cl_2]ClO_4$ (**1a**), and $[Ru(mntb)Cl_2]Cl$ (**2**) (ntb = tris(benzimidazol-2-ylmethyl)amine, mntb = tris(*N*-methylbenzimidazol-2-ylmethyl)amine) have been synthesized and characterized. The X-ray crystal structure of **1** reveals that the coordination geometry around the Ru^{III} center is distorted octahedral in which four sites are occupied by the tetradentate ligand ntb and the remaining *cis* positions by two chloride ions. The stronger $Ru–N_{bzim}$ bonds elongate the Ru–Cl bonds thereby labilizing the coordinated chloride ions. In the electronic absorption spectra the Ru^{III} complexes show two bands corresponding to $\pi(bzim) \rightarrow t_{2g}(Ru)$ and $p\pi(Cl^-) \rightarrow t_{2g}(Ru)$ ligand-to-metal charge transfer (LMCT) transitions along with intraligand transitions in the UV region. Complex **1** shows rhombic EPR spectral features (g_1, 2.238; g_2, 2.071; g_3, 1.790). The Ru^{III} complexes display both $Ru^{III} \rightarrow Ru^{II}$ reduction and $Ru^{III} \rightarrow Ru^{IV}$ oxidation processes. Complexes **1** and **2** catalyze the allylic oxidation of cyclohexene, selective and higher epoxidation of cyclooctene, and hydroxylation of alkanes in the presence of the peroxide TBHP and the peracid *m*-CPBA as cooxidants illustrating that the electronic and steric effects of tripodal 4*N* ligands can be tuned to catalyze the effective oxidative transformation of organic compounds. ESI-MS studies reveal the formation of ruthenium peroxido species in these catalytic reactions.

Introduction

Metal-catalyzed oxidations have received much attention in the recent past owing to their ability to catalyze a wide range of oxygen-transfer reactions.[1] Especially the oxidation of alkanes, which are inert to chemical conversion, has been a significant issue in bioinorganic and organic chemistry. Such reactions are catalyzed by enzymes such as heme containing cytochrome P-450 and non-heme methane monooxygenase (MMO).[2] In order to mimic these reaction systems many iron(II) and iron(III) complexes with a variety of ligands have been synthesized and their reactivity toward alkane functionalization has been investigated.[3] These oxidative transformations of organic compounds are catalyzed by the heme and non-heme enzymes and their model complexes via Fe^{IV}=O reactive intermediates.[3,4] The variation of ligand environments around the metal center plays a key role in modulating the spectral and catalytic properties. Changing the metal ion from iron to its homologous element ruthenium might lead to the formation of stable complexes and it would be interesting to explore the roles of steric and electronic factors around the metal center in the oxidation reactions.[5–11] The oxido-ruthenium(IV,V,VI) species, which are generated from the ruthenium(II/III) complexes using various oxidants, are utilized for oxygen-transfer reactions. Several ruthenium complexes of nitrogen-containing ligands have drawn much attention as oxidation catalysts and have shown high catalytic ability towards alkane oxygenation of both saturated and unsaturated hydrocarbons.[10–17] Thus the tripodal 4*N* ligand tris(pyrid-2-ylmethyl)amine (tpa, Scheme 1) and its derivatives have attracted considerable interest and metal complexes of first-row transition metals and a few second- and third-row transition metal complexes have been explored.[12,13] The tpa ligand, which includes a σ-donating tertiary amine and three π-accepting pyridine nitrogens, confers on ruthenium interesting excited-state properties[12] and also catalytic properties. Thus, Kojima et al. have reported the oxygenation of alkanes catalyzed by mono- and dinuclear ruthenium complexes $[Ru(tpa)Cl_2]ClO_4$ or $[RuCl(tpa)]_2(ClO_4)_2$ in the presence of *m*-chloroperbenzoic acid (*m*-CPBA),[14] *tert*-butyl hydroperoxide (TBHP),[15] or molecular oxygen. Masuda et al. have reported[16] ruthenium complexes of two sets of tpa-based ligands having a 6-neopentylamino or 6-pivalamide group on the pyridyl arm. When PhIO is used as an oxidant for the oxidation of different substrates the

[a] School of Chemistry, Bharathidasan University, Tiruchirappalli 620024, Tamil Nadu, India
E-mail: palani51@sify.com
palanim51@yahoo.com

amide-series complexes show relatively high epoxidation activity in comparison with those of the amine-series complexes. On the other hand, the amine-series complexes show higher reactivity for C–H bond activation and C=C bond cleavage. These complementary reactivities of ruthenium complexes, regulated by substituents at the 6 position of the tpa-type ligand, may have both a steric effect and an electronic effect on the catalytic ability. Recently, Yamaguchi et al. reported[17] the chloro(dimethyl sulfoxide)ruthenium(II) complexes of tpa and its derivatives 5-$(MeOCO)_3$-tpa, tqa [tqa = tris(2-quinolylmethyl)amine], and bpg [bpg = bis(pyrid-2-ylmethyl)glycinate]. The use of *m*-CPBA as a co-oxidant showed efficient catalytic ability towards oxidation of adamantane to 1-adamantanol with a high selectively of up to 88%.

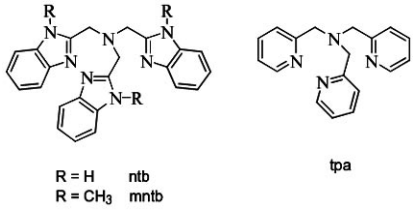

Scheme 1. Structures of tripodal ligands.

In this study we probe the effect of replacing the π-back-bonding py rings in $[Ru(tpa)Cl_2]^+$ by the more strongly σ-bonding and bulky benzimidazole (bzim) rings to obtain $[Ru(ntb)Cl_2]^+$ and $[Ru(mntb)Cl_2]^+$, where ntb is tris(benzimidazol-2-ylmethyl)amine and mntb is tris(*N*-methylbenzimidazol-2-ylmethyl)amine (Scheme 1), on the molecular structure and electronic and chemical properties and catalytic efficiency of the complexes. In fact, the copper(II)[18] and iron(III)[19,20] complexes of the ntb ligand have been isolated and studied in detail and their structures observed and the values of redox potentials measured are a clear demonstration of the predominance of steric factors over electronic contributions of the ligand. Also, Haga et al.[16] have found that the complexes with bzim skeletons can catalyze the oxidation of organic compounds. So, it is an opportunity to investigate the effect of bulky bzim pendants on the ability of the Ru^{III}–ntb complex to catalyze various oxidation reactions – hydroxylation and epoxidation – of saturated and unsaturated hydrocarbons by generating high-valent Ru-oxido species. Very recently Que et al.[21] have employed a bulky ligand to stabilize an Fe^{IV}=O complex in the solid state. The mononuclear $[Ru(ntb)Cl_2]Cl$ complex has been structurally characterized by single-crystal X-ray diffraction and it contains two axial and one equatorial bzim moieties coordinated to the metal.

Results and Discussion

Synthesis and Characterization

The dropwise addition of an ethanolic solution of the ligand ntb to a refluxing solution of $RuCl_3 \cdot 3H_2O$ in ethanol[22] led to the almost quantitative formation of the $[Ru(ntb)Cl_2]^+$ and $[Ru(mntb)Cl_2]^+$ complexes. The composition of the complexes were determined by elemental analysis (C, H, N). The Ru^{III} complexes show conductivities in acetonitrile solution revealing that they behave as 1:1 electrolytes. The FTIR spectra of the complexes display a very strong and broad band in the range 1100–1110 cm^{-1} and a strong and sharp band around 635 cm^{-1}, which are characteristic of uncoordinated ionic perchlorate. All the present Ru^{III} complexes are essentially paramagnetic. The $[Ru(ntb)Cl_2]Cl$, but not the perchlorate analogue, is highly soluble in methanol giving red-brown solutions.

Molecular Structure of $[Ru(ntb)Cl_2]Cl \cdot CH_3CN \cdot 2H_2O$ (1)

The molecular structure of the cation of complex **1** is shown in Figure 1 with 50% probability thermal ellipsoids. The coordination geometry around Ru^{III} is distorted octahedral in which four sites are occupied by the tetradentate ligand ntb and the remaining *cis* positions by two chloride ions. The bond angles around the Ru center (81.01–99.02; 162.09–179.52°) deviate considerably from the ideal values of 90° and 180° and the N4–Ru–N6 bond angle of 162.1(2)° indicates that the primary distortion involves the diagonally opposite bzim nitrogen atoms (N4, N6), which are bent away from an axis normal to the RuN1N2Cl1Cl2 plane (Figure 2).

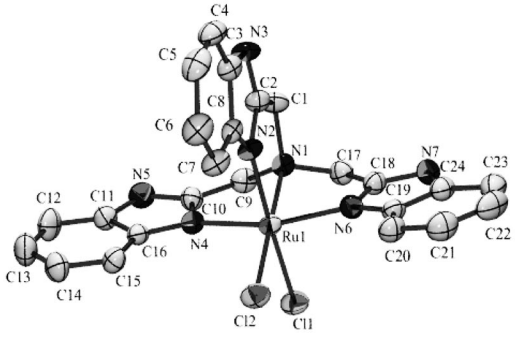

Figure 1. An ORTEP drawing of $[Ru(ntb)Cl_2]Cl$ (**1**) showing the atom numbering scheme and the thermal ellipsoids (50% probability level) for the non-hydrogen atoms. Hydrogen atoms are omitted for clarity.

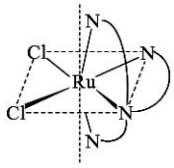

Figure 2. Illustration of the distortion of the ligand donor atoms from the octahedral positions.

Further, the coordination structure is similar to those of $[Fe(ntb)Cl_2]^+$[19,20] and $[Mn(ntb)Cl_2]$.[23] The trans Ru–N_{bzim} bonds [2.041(5), 2.047(5) Å] are shorter than the other Ru–N_{bzim} bond [2.069(4) Å]. All the Ru–N_{bzim} bonds are shorter than the Ru–N_{amine} bond [2.119(4) Å], which is expected of sp^3 and sp^2 hybrid orbitals used by the amine

and imidazole nitrogen atoms, respectively, coordinated to Ru^{III}.[20,24,25,26] Further, as the Ru^{III} center is not capable of back-bonding the metal–ligand bond lengths are determined primarily by the σ basicity of the nitrogen atoms.[27] Thus Ru–N_{bzim} bonds in **1** are shorter than the Ru–N_{py} bonds (2.073–2.087 Å)[12,14] in the analogous complex $[Ru(tpa)Cl_2]ClO_4$ (**3**) and other ruthenium complexes.[28] Similarly, the Ru–N_{im} bonds (2.020, 2.043 Å) in $[Ru(L)Cl_2](ClO_4)_2$ (**4**), where L is the tripodal ligand bis(1-methylimidazol-2-yl)methyl[2-(pyrid-2-yl)ethyl]amine, are shorter than the Ru–N_{py} bond (2.124 Å) in the same complex and also shorter than those in **3**. All these observations indicate that the bz(im) nitrogen possesses a ligand basicity that is higher and hence a σ-donor capacity better than the py nitrogen. Further, the Ru–N_{amine} (**1**, 2.119; **4**, 2.142 Å) and Ru–Cl bonds (**1**, 2.376, 2.395; **4**, 2.335, 2.379 Å) in **1** and **4** are longer than those in **3** (Ru–N_{amine}, 2.068; Ru–Cl, 2.344 Å)[12,14] revealing that the strongly σ-bonding bz(im) nitrogens labilize the Ru–N_{amine} and Ru–Cl bonds and that both im and bzim moieties have identical electronic properties. The Ru–Cl bonds in **1** are longer than those in **4** indicating that the bzim moieties in **1** exhibit a stronger steric influence on the chloride ions making them move away from ruthenium. The Cl–Ru–Cl bond angle of 88.6(1)° in **1** is lower than that in **3** (91.2°)[12,14] and **4** (94.6°)[12] because of the steric bulk of the bzim moieties in **1**, which is higher than that of the py and im moieties, leading to the pinching of the Ru–Cl bonds together and thus decreasing the Cl–Ru–Cl bond angle. Thus, it is clear that both im and bzim moieties have similar electronic properties but different steric effects with imidazole having less steric hindrance than the bzim moiety. In the crystal structure of **1** there is an extensive network of hydrogen bonds between the many possible donor and acceptor sites (Figure 3). One of the three bzim hydrogens (–NH) is hydrogen bonded to the uncoordinated chloride anion and the other two bzim –NH– nitrogens are hydrogen bonded to solvated water molecules and so on.

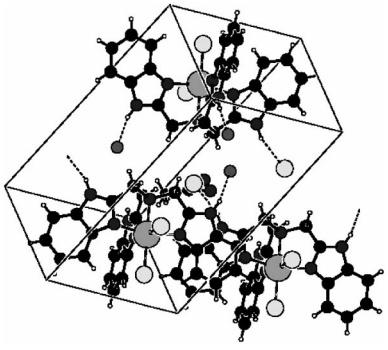

Figure 3. Unit-cell packing diagram of $[Ru(ntb)Cl_2]Cl\cdot CH_3CN\cdot 2H_2O$ (**1**) showing the network of hydrogen bonds.

Electronic Spectral Properties

For the Ru^{III} complexes the strong absorption band around 430 nm (Figure 4), which is responsible for the red-dish-brown color of the complexes, and the less intense one around 535 nm probably originate[12] from $\pi_{bzim} \rightarrow t_{2g}(Ru)$ ligand-to-metal charge transfer (LMCT) transitions. The shoulder around 325 nm may originate from the $p_\pi(Cl^-) \rightarrow t_{2g}(Ru)$ LMCT transition.[29,30] The rhombic EPR spectra of **1a** and **2** in MeOH/acetone (4:1 v/v) glass at 77 K (Figure 5, Table 1) are characteristic of low-spin (S = 1/2) Ru^{III} complexes with a distorted octahedral environment.[31–39] The analysis[40] of the EPR spectra using the *g*-tensor theory of low-spin d^5 ions provides the axial (Δ) and rhombic (*V*) components of distortion around Ru^{III} (Figure 4, Table 1) as well as the energies of the two crystal-field transitions (ν_1 and ν_2) from ground to upper Kramer's doublets.[31–33] In this analysis the combination, g_1 and g_2 negative, g_3 positive, and $g_1 > g_2 > g_3$, gave a reasonable value of k (<1.0). In these complexes the axial distortion (Δ/λ) is approximately 2.3 times more than the rhombic distortion

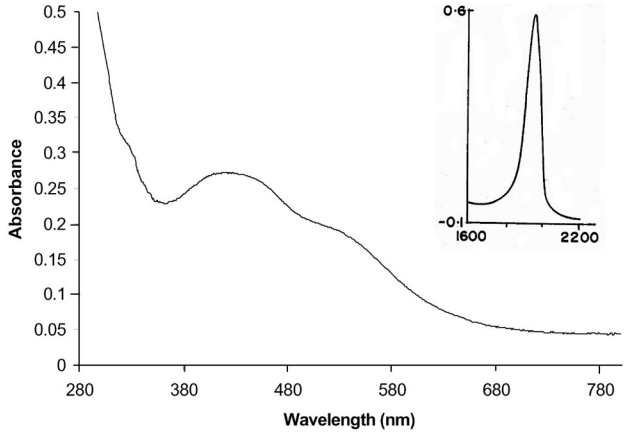

Figure 4. Electronic spectrum of the complex $[Ru(ntb)Cl_2]ClO_4$ (**1a**) (concd., 1.8×10^{-4} M) in acetonitrile solution. Inset shows the electronic spectrum of **1a** (concd., 5.4×10^{-3} M) in the range 2200–1600 nm.

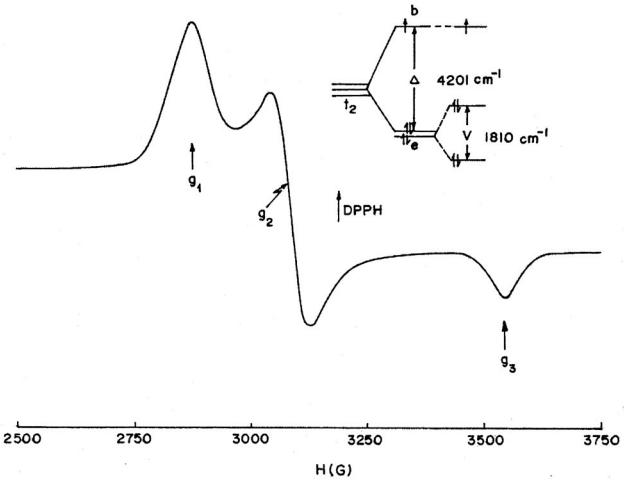

Figure 5. EPR spectrum of $[Ru(ntb)Cl_2]ClO_4$ (**1a**) in methanol/acetone (4:1 v/v) glass at 77 K. Inset shows the splitting of the t_{2g} orbitals.

(V/λ), which is consistent with the observation for the *trans* Ru–N_{bzim} bond distances, which are shorter than the equatorial Ru–N_{bzim} distance in the X-ray crystal structure of **1**.

Table 1. The EPR g values[a] and distortion parameters[b,c] of the ruthenium(III) complexes.

	1	**1a**
g_1	–2.2379	–2.2463
g_2	–2.0710	–2.1002
g_3	1.7901	1.8193
a	0.2052	0.1892
b	0.9778	0.9814
c	0.0417	0.0354
k	0.4266	0.4710
Δ/λ	3.9087	4.2009
V/λ	–1.8522	–1.8099
v_1/λ	3.1259	3.4142
v_2/λ	5.1368	5.3996

[a] In methanol/acetone (4:1, v/v) solution at 77 K. [b] Orbital reduction factor (k), axial distortion (Δ/λ), rhombic distortion (V/λ) and ligand-field transitions (v_1/λ, v_2/λ). [c] A second solution having small distortions where both v_1 and v_2 values also exist but are eliminated as unacceptable as they are inconsistent with the experimentally observed near-IR spectroscopic results.

Electrochemical Studies

The Ru^{III} complexes **1**, **1a**, and **2** show an irreversible Ru^{III}–Ru^{II} redox process ($E_{1/2}$, –0.400 to –0.445 V; ΔE_p, 200–274 mV) and a quasi-reversible Ru^{III}–Ru^{IV} redox process ($E_{1/2}$, 1.16 V; ΔE_p, 120–140 mV, Table 2, Figure 6). The effect of incorporating the N–Me group as in **2** shifts the Ru^{III}/Ru^{II} redox potential to more negative values on account of the electron-releasing methyl group rendering the reduction of Ru^{III} difficult. The observed irreversibility of the Ru^{III}–Ru^{II} redox process for **1a** is in contrast to the reversibility of that for the py analogue $[Ru(tpa)Cl_2]ClO_4$ (**3**). The replacement of the labile chloride (cf. molecular structure description) by solvent on electrochemical reduction leads to the formation of the solvated $[Ru(ntb)(Cl)(MeOH)]^+$ species, which undergoes facile reoxidation at a potential more positive than that expected for $[Ru(ntb)Cl_2]$, and hence the higher ΔE_p observed. For **1a** the Ru^{III}/Ru^{II} redox potential is more negative and the Ru^{III}/Ru^{IV} redox potential less positive than those (–0.13, 1.37 V)[12,14] for **3**. This indicates that the strongly σ-donating bzim nitrogens in **1a** stabilize the higher Ru^{III} and Ru^{IV} oxidation states much better than the pyridine nitrogens in **3** do.

Table 2. Redox properties of ruthenium(III) complexes[a] in methanol at 25 ± 0.2 °C.

	E_{pc} [V]	E_{pa} [V]	ΔE_p [mV]	$E_{1/2}$ [V]	$E_{1/2}$[b] [V]	i_{pc}/i_{pa}	$D \times 10^6$ [$cm^2\ s^{-1}$]	Redox Process
1	–0.502	–0.298	204	–0.400	–0.429	0.76	4.2	Ru^{III}/Ru^{II}
	1.088	1.228	140	1.158	1.147	0.81	7.6	Ru^{III}/Ru^{IV}
1a	–0.537	–0.263	274	–0.400	–0.443	0.83	4.0	Ru^{III}/Ru^{II}
	1.096	1.216	120	1.156	1.135	0.75	7.9	Ru^{III}/Ru^{IV}

[a] Measured vs. non-aqueous Ag/Ag^+ reference electrode; scan rate, 50 mV s^{-1}; supporting electrolyte, $[(C_4H_9)_4N](ClO_4)$ (0.1 M). [b] Differential pulse voltammetry, scan rate, 1 mV s^{-1}; pulse height, 50 mV.

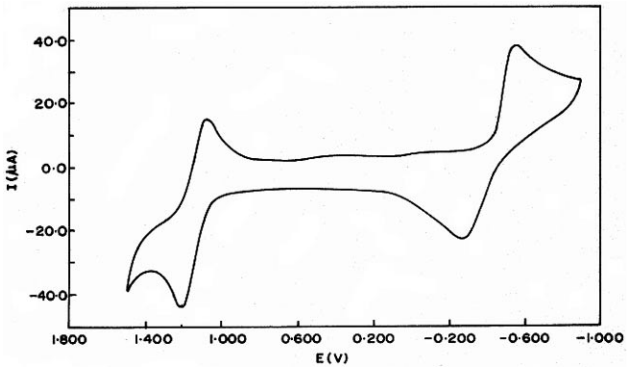

Figure 6. Cyclic votammogram of complex $[Ru(ntb)Cl_2]ClO_4$ (**1a**) (0.001 M) in CH_3CN at 25 °C at 0.05 V s^{-1} scan rate.

Catalytic Oxidations of Hydrocarbons with [Ru(ntb/mntb)-Cl_2]Cl

The Ru^{III} complexes of tripodal tpa ligands with pivalamide substituents on the pyridyl rings show catalytic epoxidation activity that is higher than that for the Ru^{II} complexes of tpa ligands with neopentylamine substituents, while the latter complexes show a catalytic activity for hydroxylation, allylic oxidation, and C=C bond cleavage reactions higher than that for the former through the involvement of oxido-ruthenium(V) species generated in the presence of PhIO as oxidant.[16,41] In the present study the effect of replacing the pyridyl pendants in $[Ru(tpa)Cl_2]Cl$ by bzim pendants on the catalytic activities of $[Ru(ntb)Cl_2]^+$ (**1**) and its *N*-methyl analogue $[Ru(mntb)Cl_2]^+$ (**2**) has been explored. The complexes **1** and **2** show catalytic activity towards allylic oxidation, epoxidation, and alkane hydroxylation in the presence of the peroxide TBHP and the peracid *m*-CPBA as cooxidants in methanol solution (Scheme 2, Table 3, Table 4). These oxidants are known[41] to be potentially strong in generating high-valent Ru^V=O active species from Ru^{III} complexes for oxygen-transfer reactions. When a methanolic solution of **1** is treated with *m*-CPBA the band around 534 nm (ε = 1040 $M^{-1}\,cm^{-1}$) disappears and that around 428 nm (ε = 1510 $M^{-1}\,cm^{-1}$) is shifted to around 414 nm (ε = 1090 $M^{-1}\,cm^{-1}$) with its intensity reaching a maximum within a few minutes. Also, the ESI-mass spectrum of a methanolic solution of **1** and 100 equiv. of *m*-CPBA after 1 h of mixing shows prominent peak clusters at *m*/*z* values of 713 and 804 corresponding to the peroxido species $[Cl(ntb)Ru–O–O–CO–C_6H_4Cl]^+$ and its solvated adduct $[(MeOH)_2(H_2O)_3Cl(ntb)Ru–O–O–CO–C_6H_4Cl]^+$, respectively. When TBHP is used in place of the *m*-CPBA similar spectral changes are observed but with the intensity of the band around 414 nm (ε, 1560 $M^{-1}\,cm^{-1}$) reaching a maximum over a period of 7 h. This suggests the formation of the peroxido species $[Cl(ntb)Ru–O–O–t\mathrm{Bu}]^+$

as the reaction intermediate, similar to that obtained for the addition of *m*-CPBA. The formation of the peroxido species is in sharp contrast to the direct formation[16,41] of the high-valent $[Ru^{V}(tpa\text{-}based)(O)(Cl)]^{2+}$ species from $[Ru(tpa\text{-}based)Cl_2]Cl$ on treatment with the PhIO cooxidant as detected by ESI-MS. Also, interestingly, the complex $[Ru^{V}(L)(O)](ClO_4)_2$ {HL = [2-hydroxy-(2-pyridyl)ethyl]bis-[2-(2-pyridyl)ethyl]amine} has been isolated and is found to be a very active stoichiometric oxidant towards hydrocarbons.[42] For the present complexes **1** and **2** the peroxido species are stabilized by incorporating bulky and strongly σ-donating bzim moieties in place of the py pendants in the analogous $[Ru(tpa)Cl_2]^{+}$ complex. This is supported by the observation of $Ru^{III} \rightarrow Ru^{IV}$ oxidation for **1** and **2** at poten-

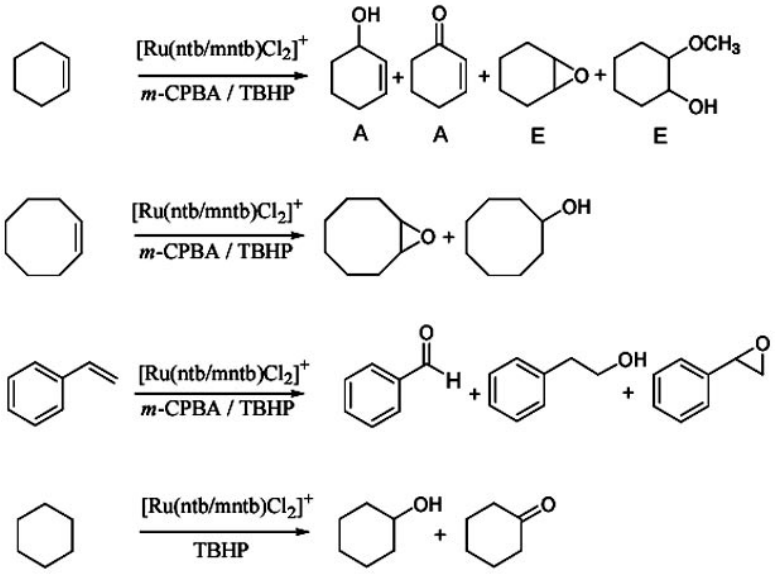

Scheme 2. Various oxidative transformations catalyzed by **1** and **2**.

Table 3. Oxidation of alkanes/alkenes by $[Ru(ntb)Cl_2]Cl$ (**1**).[a]

Substrate	Products	*t*BuOOH (air)			*t*BuOOH (N_2)			*m*CPBA		
		Yield[c] [%]	TON[b]	A/E	Yield[c] [%]	TON[b]	A/E	Yield[c] [%]	TON[b]	A/E
Cyclohexene[b]	2-cyclohexen-1-ol (A)	26.4	264	1.0	25.5	255	3.3	26.1	261	0.9
	2-cyclohexen-1-one (A)	0.8	8		28.7	287		3.9	39	
	1,2-epoxycyclohexene (E)	14.6	146		3.3	33		13.8	138	
	2-methoxy-1-cyclohexanol (E)	11.3	113		6.9	69		21.1	211	
	cyclohexane-1,2-diol (E)	trace	–		6.4	64		–	–	
Cyclohexene[d]	2-cyclohexen-1-ol (A)	0.3	–	–	1.2	–	–	3.1	–	–
	2-cyclohexen-1-one (A)	0.7	–		0.8	–		1.6	–	
	1,2-epoxycyclohexene (E)	0.6	–		10.8	–		4.7	–	
Cyclooctene	1,2-epoxycyclooctene	15.9	159	0.5	1.2	11	0.7	20.4	204	0.3
	cyclooctanol	8.2	83		0.4	4		5.9	59	
	2-cycloocten-1-one	–	–		0.4	4		–	–	
Styrene	benzaldehyde	8.8	89		32.8	328		2.9	29	
	1-phenyloxirane	trace	1		1.6	16		3.5	35	
	2-phenylethanol	13.3	133		–	–		8.3	83	
Cyclohexane	cyclohexanol	0.86	9					trace	–	
	cyclohexanone	0.51	5					–	–	
Tetrahydrofuran	tetrahydrofuran-2-ol	trace	–					–	–	
	γ-butyrolactone	2.7	27					0.6	6	
	3-hydroxypropionic acid	1.6	14					0.9	9	
	2-methoxytetrahydrofuran	–	–					1.0	10	
Ethylbenzene	1-phenylethanol	1.0	10		1.0	10		trace	–	
	acetophenone	0.4	4		3.2	32		0.6	6	
Toluene	benzaldehyde	0.8	8					0.8	8	
Cumene	acetophenone	trace	–		1.2	12		–	–	
	2-phenyl-2-propanol	–	–		1.9	20		–	–	

[a] Reaction conditions: alkanes/alkenes (1.0 M), complex (1.0×10^{-4} M), *t*BuOOH/*m*-CPBA/H_2O_2 (1.0×10^{-1} M), CH_3OH (5 mL), temperature 25 °C, time 12 h. [b] TON = mol product/mol catalyst. [c] Yield based on the substrate, average of 3 runs. [d] Control reaction without catalyst.

Table 4. Catalytic oxidation of alkanes/alkenes by [Ru(mntb)Cl_2]Cl (**2**) in the presence of N_2.[a]

Substrate	Products	*t*BuOOH Yield[c] [%]	TON[b]	A/E	*m*-CPBA Yield[c] [%]	TON[b]	A/E
Cyclohexene	2-cyclohexen-1-ol (A)	21.2	212	0.3	32.7	327	0.5
	1,2-epoxycyclohexene (E)	1.8	18		9.5	95	
	2-methoxy-1-cyclohexanol (E)	8.3	83		17.4	174	
	cyclohexane-1,2-diol (E)	7.0	70		7.5	75	
	2-cyclohexen-1-one (A)	36.4	364		35.4	355	
Cyclooctene	cyclooctanol	12.4	124	1.3	12.9	129	0.4
	1,2-epoxycyclooctene	14.1	141		33.7	337	
	2-cycloocten-1-ol	2.6	26		–	–	
	2-cycloocten-1-enone	3.8	34		–	–	
Styrene	benzaldehyde	35.0	350		2.0	20	
	1-phenyloxirane	7.7	1		3.9	39	
Cyclohexane	cyclohexanol	0.4	4		trace	–	
	cyclohexanone	0.6	6		–	–	
	chlorocyclohexane	1.2	12				
Ethylbenzene	1-phenylethanol	4.3	43		0.1	1	
	acetophenone	17.4	173		0.8	8	
Cumene	2-phenylpropan-ol	9.9	99		0.7	7	
	acetophenone	3.1	31		0.2	2	

[a] Reaction conditions: alkanes/alkenes (1.0 M), complex (1.0×10^{-4} M), *t*BuOOH/*m*-CPBA/H_2O_2 (1.0×10^{-1} M), CH_3OH (5 mL), temperature 25 °C, time 12 h. [b] TON = mol product/mol catalyst. [c] Yield based on the substrate, average of 3 runs.

tials less positive than $[Ru(tpa)Cl_2]^+$ (cf. above). These peroxido species are assumed to be directly involved in oxidation reactions as they do not decompose to generate the high-valent species[16,41,43] $[(ntb/mntb)(Cl)Ru^{V}{=}O]^{2+}$ or $[(ntb/mntb)Ru^{V}{=}O]^{3+}$ (see Schemes 3, 4, and 5) for effecting the catalytic oxidation reactions.

The yields of products of oxidations catalyzed by **1** and **2** are modest on account of the catalyst containing a substitutionally inert chloride ligand[44] and bulky bzim pendants, which render the approach[16] of substrates towards the catalyst difficult. When treated with hydrogen peroxide **1** and **2** fail to generate the hydroperoxido intermediate as seen from a UV/Vis spectral study and no catalytic oxidation of alkanes is observed, which can be attributed to the formation of an inactive catalyst.[45]

Cyclohexene Oxidation

The oxidation of all the organic substrates was carried out in methanol as the solvent at room temperature under both aerobic and anaerobic conditions over 12 h. In the presence of TBHP complex **1** effects the allylic oxidation of cyclohexene to provide 2-cyclohexene-1-ol (A, 26.4%) and 2-cyclohexene-1-one (A, 0.8%), which is the further oxidized product of the former involving a dehydrogenation pathway[16,46] catalyzed by **1**. In addition, the epoxidation product 1,2-epoxycyclohexene (E), obtained in yields lower than the allylic oxidation products, undergoes nucleophilic attack by hydroxide and methoxide ions in methanol solution to give the cleavage compounds cyclohexane-1,2-diol (E, traces) and 2-methoxy-1-cyclohexanol (E, 11.3%), respectively. Similar results are obtained when *m*-CPBA is used as the cooxidant. This is in contrast to the formation of epoxide in major amounts and allylic oxidation products in small amounts when the analogous $[Ru(tpa\text{-based})Cl_2]^+$ complexes are used as the catalysts in the presence of PhIO as the cooxidant.[16] Thus, the A/E ratio is enhanced from 0.05–0.83 for the tpa-based complexes to 0.9 (*m*-CPBA) and 1.0 (TBHP) for **1**. Also, complex **2**, the *N*-methylated analogue of **1**, yields increased amounts of allylic oxidation products and decreased amounts of epoxidation products (A/E ratio: TBHP, **1**, 1.0, **2**, 0.3; *m*-CPBA, **1**, 0.9; **2**, 0.5). This is interesting because TBHP and *m*-CPBA are well known to facilitate epoxidation reactions[16] even in the absence of a catalyst. Masuda et al. have suggested that the epoxidation activity of Ru(tpa-based) complexes involves the abstraction of the allylic proton by the high-valent $Ru^{V}{=}O$ species generated by PhIO,[16,41] followed by a rapid in-caged one-electron transfer before the alkenyl radical intermediate R and Ru^{V}–OH diffuse into solution.[46–48] Meyer et al. have argued that the $Ru^{IV}{=}O$ species prefers an attack on the allylic C–H rather than on the olefin double

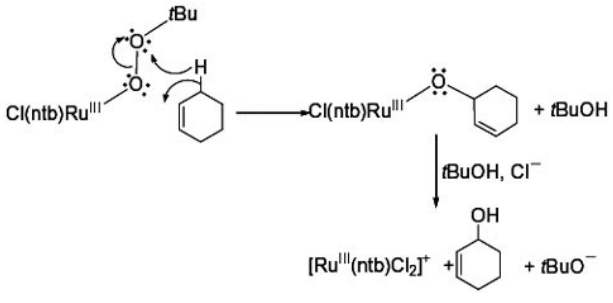

Scheme 3. Proposed mechanism for allylic oxidation using TBHP.

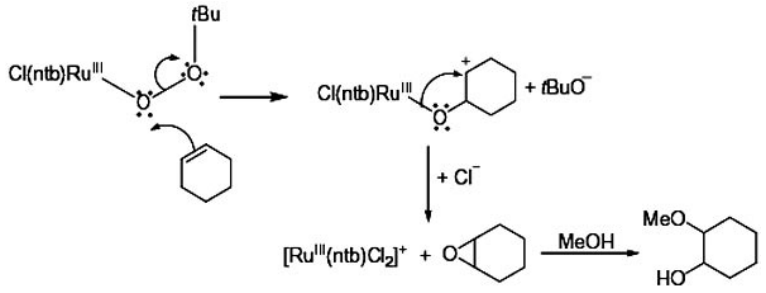

Scheme 4. Proposed mechanism for epoxidation using TBHP.

bond,[46] which is followed by rapid comproportionation of the intermediate to give the Ru^{III} species. So, for the complexes **1** and **2** we propose that the peroxido species $[Cl(ntb)Ru–O–O–tBu]^+$ directly attacks the allylic C–H bond (Scheme 3) to form the alkoxido Ru^{III} species $[Cl(ntb)Ru–O–C_6H_9]^+$ through heterolysis of the peroxido bond in the intermediate. The latter reacts with *t*BuOH and a chloride ion to yield the allylic alcohol product and regenerate the original complex. The alkylperoxido intermediate attacks the olefinic double bond, such as the $Ru^{V}=O$ species,[46] to yield a carbo cation, which collapses to a Ru^{III} species upon attack of the chloride ion (or solvent molecule) to yield the epoxide and regenerate the original complex (Scheme 4). Further, the strong σ-bonding and weakly π-accepting nature of bulky benzimidazole moieties in **1** and **2** facilitate the heterolysis of the O–O bond in the reaction intermediate $[Cl(ntb)Ru–O–O–tBu]^+$.

It is well established that autoxidation of cyclohexene by *m*-CPBA, even in the absence of a catalyst, occurs through free radical chain reactions[49] to yield 2-cyclohexen-1-ol, 2-cyclohexen-1-one, and 1,2-epoxycyclohexane in the presence of oxygen. Thus, control experiments for cyclohexene oxidation without the catalyst gave the total yield (epoxide, alcohol, and ketone) of only 3–5% for *m*-CPBA and <1% for TBHP as cooxidants under aerobic conditions and the yields (2-cyclohexen-1-ol; 1.2%, 2-cyclohexen-1-one; < 1%, and 1,2-epoxycyclohexane; 10.8%) are higher under anaerobic (N_2) conditions revealing the possibility of autoxidation of cyclohexene in the presence of oxygen. On the other hand, the yields of these products obtained in the presence of the catalysts **1** and **2** are much higher (50–75%) suggesting that both the complexes catalyze the oxidation reactions and that the solvent methanol may retard the reactions by competing for the coordination positions of the active metal species.[50] Further, when the reaction mixtures containing the catalysts and TBHP are deaerated with N_2 the yields of epoxidation products of cyclohexene decrease and the allylic oxidation products increase with the A/E ratio increasing from 1.1 to 3.3 and the total yield enhancing from 53 to 71%. This confirms the presence of autoxidation in methanol as solvent and provides strong evidence for metal-catalyzed allylic oxidation and epoxidation reactions. Similar enhanced allylic oxidation products (Table 4) were also obtained for **2**, the *N*-methyl analogue of **1**, revealing that allylic oxidation is favored by the bzim complexes. Further, **2** appears to be much better than **1** for allylic oxidation with higher A/E ratios in a nitrogen atmosphere, and for further oxidation of 2-cyclohexen-1-ol to 2-cyclohexen-1-one in the presence of TBHP. Also for *m*-CPBA the A/E ratio is increased from 0.9 to 2.0. It is also revealed that exclusion of oxygen is crucial for increasing the selectivity for allylic oxidation. Further, for the cyclohexene oxidation with TBHP, addition of water increases the yield of the epoxide by up to 0.9%, effects almost no change in that of 2-cyclohexen-1-ol, and decreases the yield of the allylic oxidation product 2-cyclohexen-1-one by up to 0.8%. Thus the present catalysts **1** and **2** have the potential to be developed into selective allylic oxidation catalysts using TBHP rather than *m*-CBPA as the cooxidant in a non-aqueous solvent.

Cyclooctene Oxidation

The epoxidation of cyclooctene to give 1,2-epoxycyclooctane and cyclooctanol is selectively catalyzed by **1** through the heterolytic cleavage of the peroxido intermediate (Scheme 4) and the cyclooctanol results from the reduction of the epoxide by the methanol solvent. But, when the reaction mixture is deaerated with nitrogen the yield of the epoxidation product 1,2-epoxycyclooctane decreases enormously suggesting the role of autoxidation under aerobic conditions. However, the yields are higher and also the TONs are three times higher than that of the analogous $[Ru(tpa)Cl_2]^+$ complex.[16] Further, the catalyst **2** is much better than **1** for epoxidation of cyclooctene under anaerobic conditions in terms of higher yields; however, the epoxidation has lower selectivity (A/E, 1.3) than the allylic oxidation products when TBHP is used as the cooxidant. Interestingly, *m*-CPBA is found to be a very selective and better cooxidant than TBHP for epoxidation catalyzed by **2**, which does not contain the reactive N–H group.

Styrene Oxidation

Styrene is catalytically epoxidized by **1** under aerobic conditions to provide 1-phenyloxirane (traces), 2-phenylethanol, and benzaldehyde with the peroxide TBHP giving a higher TON than *m*-CPBA. The product 2-phenylethanol is expected to be formed by the attack of the methanol solvent on the epoxide obtained by the attack of the alkylper-

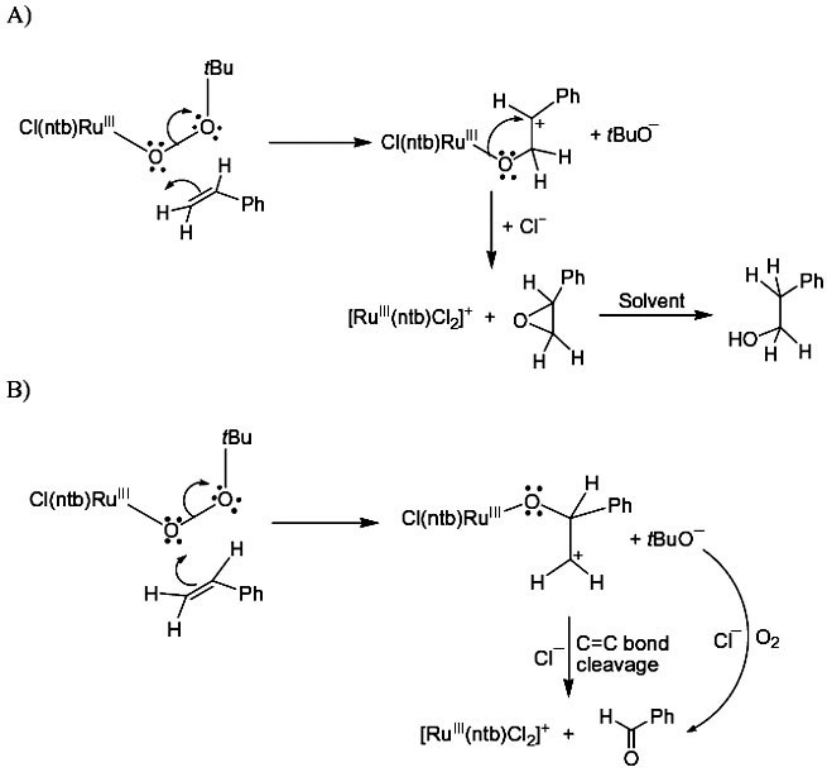

Scheme 5. Proposed mechanisms for the oxidation of alkene (styrene).

oxido intermediate on the olefinic double bond of styrene (Scheme 5, A). The amount of benzaldehyde detected in the N_2 atmosphere is lower than that in the presence of oxygen supporting its formation through further oxidation of the carbo cation directly by oxygen or through C=C cleavage[47] in the absence of oxygen (Scheme 5, B). The product phenylethanol is not detected under nitrogen for **1** and also for **2** even in the presence of oxygen, suggesting the involvement of oxygen and the (bzim)N–H group (**1**) in its formation.

Alkane Oxidation

The catalytic activity of **1** and **2** towards alkane functionalization was also examined using cyclohexane, THF, ethylbenzene, toluene, and cumene as typical substrates in the presence of both TBHP and *m*-CPBA as cooxidants. Catalytic oxidations under a nitrogen atmosphere gave similar results and TBHP was found to be a better cooxidant than *m*-CPBA. Control reactions without **1** and **2** as catalysts fail to effect any significant oxidative transformations of alkanes in the presence of both *m*-CPBA and TBHP revealing that the reactions are only metal-catalyzed. In the presence of TBHP cyclohexane is oxidized to cyclohexanol (A) (Scheme 2) and further to cyclohexanone (K). The yields are lower but the TONs are almost the same as those observed for the analogous $[Ru(tpa\text{-}based)Cl_2]^+$ complexes.[14,16,42] Interestingly, in contrast to the $[Ru(tpa)Cl_2]^+$ and $[Fe(tpa)Cl_2]^+$ complexes,[13,14] no chlorinated product is obtained for **1**. This indicates that the reaction intermediate involved in oxygen transfer is $[Cl(ntb)Ru–O–O–tBu]^+$ rather than the putative and sterically hindered [Ru(Cl)(O)(ntb)] species, which would have otherwise been responsible for the chloride transfer[14,16] as observed for [Ru(Cl)(O)(tpa)]. The mechanistic pathway for the oxidation of alkanes by $[Ru(ntb/mntb)Cl_2]^+$ is suggested to involve the peroxido species $[Cl(ntb)Ru–O–O–tBu]^+$ as reaction intermediates (cf. above). The latter attacks the alkane directly, followed by heterolysis of the O–O bond to give the alkoxido ruthenium species $[Cl(ntb)Ru–O–CH_2–]^+$, which reacts with H^+ and $Cl^–$ to give the hydroxylated product and regenerate the catalyst (Scheme 6). The observation of an *A*/*K* value of 1.8 supports the heterolytic cleavage of the O–O bond in the peroxido intermediate and the noninvolvement of a free radical mechanism. However, the *A*/*K* value obtained (0.6) for **2** under N_2 is lower and the addition of 2,6-di-*tert*-butyl-4-methylphenol (BHT) as a radical trapping agent to the oxidation reaction of cyclohexane catalyzed by **1** and **2** using TBHP yields no BHT oxidation product, illustrating the noninvolvement of a radical mechanism. Chlorobenzene has been detected in very small quantities as one of the products in cyclohexane oxidations supporting our proposal of heterolytic O–O bond cleavage of the active species $[Cl(ntb)Ru–O–O–CO–C_6H_4Cl]^+$. Interestingly, chlorocyclohexane, in addition to cyclohexanol and cyclohexanone, has been detected in good yield for **2** indicating that the active species is $[Cl(ntb)Ru–O–O–tBu]^+$ rather than [Ru(O)-(mntb)].

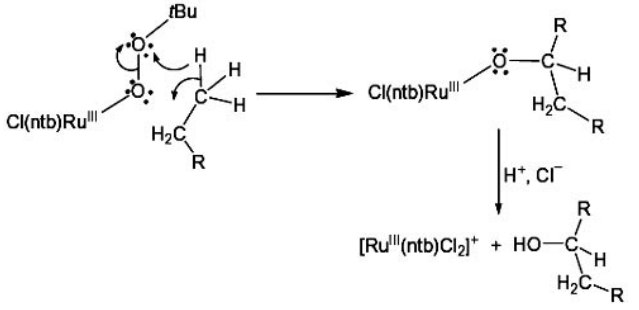

Scheme 6. Proposed mechanistic pathway for the catalytic oxidation of alkanes.

In the case of THF as substrate traces of the hydroxylated product tetrahydrofuran-2-ol is detected and higher amounts of the further oxidized product γ-butyrolactone is preferentially obtained. On hydrolysis the latter provides 4-hydroxybutyric acid, which then undergoes decarboxylation[49] to give the 3-hydroxypropyl radical followed by its facile catalytic oxidation to 3-hydroxypropionic acid. Toluene preferentially yields the further oxidized product benzaldehyde. It is obvious that the complexes **1** and **2** can oxidize toluene first to benzyl alcohol (Scheme 6) and then to benzaldehyde, the oxidation of benzyl alcohol to benzaldehyde is expected to be 200 times faster than that of toluene to benzyl alcohol.[48] The secondary C–H bond of ethylbenzene is selectively oxidized to give the hydroxylated product 1-phenylethanol, which undergoes dehydrogenation catalyzed by **1** and **2** to provide acetophenone. Also the selective oxidation of tertiary C–H bonds of cumene to give 2-phenyl-2-propanol and the further oxidized product acetophenone has been observed.

We propose that $[Cl(ntb)Ru–O–O–tBu]^+$ rather than the $[(ntb)Ru^{IV}=O]^{2+}$ species is the active intermediate (Scheme 6) involved in the hydroxylation reactions. Chlorobenzene has been detected in very small quantities as one of the products in both cyclohexene and cyclohexane oxidations and the methoxide ion formed enhances the yield of 2-methoxy-1-cyclohexanol when *m*-CBPA is used for cyclohexene oxidation, supporting our proposal. However, interestingly, chlorocyclohexane, in addition to cyclohexanol and cyclohexanone, has been detected in good yield for **2** indicating that the active species is [Ru(Cl)(O)(mntb)] rather than [Ru(O)(mntb)]. The electron-releasing *N*-methyl groups are expected to stabilize the higher oxidation states of metal ions and hence their interaction with chloride anions. The electron-donating and bulky bzim pendants are expected to stabilize the intermediate $Ru^{IV}=O$ species leading to enhanced oxidation activities by **1**; however, the bulkiness of the bzim moiety would hinder the approach of the substrate causing a decrease in hydroxylation activity. It is interesting that allylic oxidation is favored for cyclohexene while epoxidation is favored for cyclooctene and styrene. This illustrates that the catalytic oxidation activity of the tripodal ligand complex is controlled and tuned by electronic as well as steric factors around the metal center.

Conclusions

We have described here the synthesis, characterization, and catalytic behavior of monomeric Ru^{III} complexes of the sterically constrained tripodal tetradentate ligands tris(benzimidazol-2-ylmethyl)amine (ntb) and its NMe derivative (mntb). The X-ray crystal structure of $[Ru(ntb)Cl_2]^+$ indicates that the steric constraints of the tripodal ligand with bulky bzim moieties cause geometric distortion in the octahedral coordination sphere of Ru^{III}, which is consistent with the EPR and near-IR spectra. The incorporation of the sterically hindered and strongly σ-donating and weakly π-accepting bzim rings as in $[Ru(ntb)Cl_2]^+$ and $[Ru(mntb)Cl_2]^+$ facilitates the formation of $[Cl(ntb/mntb)Ru–O–O–CO–C_6H_4Cl]^+$ and $[Cl(ntb/mntb)Ru–O–O–tBu]^+$ species responsible for oxidation activity. Interestingly, allylic oxidation is favored for cyclohexene while epoxidation is favored for cyclooctene and styrene. The Ru^{III} complexes have the potential to be developed into a selective and efficient catalyst for allylic oxidation, epoxidation, and alkane functionalization.

Experimental Section

General: $RuCl_3·3H_2O$ was obtained from Arora–Mathey Ltd. The ligand tris(benzimidazol-2-ylmethyl)amine (ntb)[51] and tris(*N*-methylbenzimidazol-2-ylmethyl)amine (mntb)[52] were synthesized by using a published procedure. All the common chemicals were of reagent grade and were used as received. Reagent grade solvents were dried and distilled by usual methods and the solvents were stored over molecular sieves (4 Å). Tetra-*N*-ethylammonium perchlorate (TEAP) was prepared from tetra-*N*-ethylammonium bromide (G. F. Smith, USA) by a standard procedure.[53] Cyclohexene was purified by passing it through a column of alumina to remove the BHT (2,6-di-*tert*-butyl-4-methylphenol) stabilizer followed by fractional distillation. The purity of the other substrates were checked by gas chromatography before use.

Physical Measurements: The elemental analyses were performed at the Central Drug Research Institute (CDRI), Lucknow, India. The solution electrical conductivity was obtained using a Systronic 305 conductivity bridge. The IR spectra of the complexes (400–4000 cm^{-1}) were measured with a Perkin–Elmer Spectrum One FT-IR spectrophotometer. The electronic spectra were recorded using a Hitachi U3410 double beam UV/Vis/NIR spectrophotometer. The ^1H spectra were obtained at room temperature using a Bruker 400 MHz spectrometer. The chemical shift values in $[D_6]$DMSO are reported with respect to tetramethylsilane as internal standard and the values are reported as: δ values (multiplicity, assignment). The EPR spectra were obtained with a Varian E-112 X-band spectrometer, the field being calibrated with diphenylpicrylhydrazyl (DPPH). The *g* values were derived for the 77 K spectra. ESI-mass spectra for characterization of the intermediate ruthenium species in a methanol solution was obtained with a Q-top Micro ESI-Mass spectrophotometer. Cyclic voltammetry and differential pulse voltammetry with a platinum sphere electrode were performed at 25 ± 0.2 °C. The temperature of the electrochemical cell was maintained by a cryocirculator (HAAKE D8-G). Voltammograms were generated with the use of a EG&G PAR Model 273 potentiostat. A Pentium IV computer along with EG&G M270 software was used to control the experiments and acquire the data. A three-electrode system consisting of a platinum sphere (0.287 cm^2), a plati-

num auxiliary electrode, and a reference electrode was used. The reference electrode for the non-aqueous solution was $Ag(s)/Ag^+$, which consisted of a Ag wire immersed in a solution of $AgNO_3$ (0.01 M) and tetra-*N*-hexylammonium perchlorate (0.1 M) in acetonitrile placed in a tube fitted with a vycor.[54] The $E_{1/2}$ and ΔE_p observed under identical conditions for the Fc/Fc^+ couple in acetonitrile was 0.100 V and 76 mV, respectively, with respect to the Ag/Ag^+ reference electrode. The cyclic voltammograms (CV) and differential pulse voltammograms (DPV) were obtained in CH_3OH/CH_3CN solutions with 0.1 M $[(C_4H_9)_4N]ClO_4$ as the supporting electrolyte at ambient temperatures under N_2. Redox potentials were measured relative to a Ag/Ag^+ reference electrode. All the complexes are electroactive with respect to the metal as well as the ligand centers over the potential range ±2 V.

Synthesis of Complexes

$[Ru(ntb)Cl_2]Cl$ (1): Ntb (0.41 g, 1 mmol) in ethanol (20 mL) was added to a solution of $RuCl_3·3H_2O$ (0.26 g, 1 mmol) heated at reflux in ethanol (80 mL). The mixture was further heated at reflux for 12 h. The color of the solution changed from brown to red brown. The red-brown solution was filtered while hot and concentrated to 30 mL. The concentrated solution was kept at 5 °C and the resulting red-brown crystalline precipitate was filtered off and dried in vacuo giving a yield of ca. 75% (0.46 g). A single crystal of compound **1** was obtained by recrystallizing it from a 2 M HCl solution. $C_{24}H_{21}N_7Cl_3Ru$ (**1**): calcd. C 46.88, H 3.44, N 15.95; found C 47.21, H 3.73, N 16.04. Λ_M = 142 Ω^{-1} cm^2 mol^{-1}. UV/Vis (CH_3OH): λ_{max} (ε, $M^{-1}cm^{-1}$) = 534 (1040), 428 (1510), 325 (sh), 275 (25470), 240 (sh) nm.

$[Ru(ntb)Cl_2]ClO_4$ (1a): $[Ru(ntb)Cl_2]Cl$ (**1**) (0.31 g, 0.5 mmol) was dissolved in methanol (25 mL) and a saturated aqueous solution of $NaClO_4$ was added, and the solution was stirred vigorously for 10 min. A reddish-brown crystalline precipitate was isolated by slow evaporation at room temperature, filtered off, and dried in vacuo giving ca. 71% (0.46 g) yield. $C_{24}H_{21}Cl_3N_7O_4Ru$ (678.90): calcd. C 42.46, H 3.12, N 14.44; found C 42.79, H 2.98, N 14.28. Λ_M = 151 Ω^{-1} cm^2 mol^{-1}. IR (KBr disk): $\tilde{\nu}$ = $\nu(ClO_4^-)$, 1100, 610 cm^{-1}. UV/Vis (CH_3CN): λ_{max} (ε, $M^{-1}cm^{-1}$) = 530 (1060), 425 (1540), 325 (sh), 275 (25360), 235 (sh) nm.

$[Ru(mntb)Cl_2]Cl$ (2): The procedure used for **1** was employed for isolating **2** in 82% yield. $C_{27}H_{27}Cl_3N_7Ru$ (656.99): calcd. C 49.36, H 4.14, N 14.92; found C 49.37, H 4.13, N 14.94. Λ_M = 142 Ω^{-1} cm^2 mol^{-1}. UV/Vis (CH_3OH): λ_{max} (ε, $M^{-1}cm^{-1}$) = 537 (1075), 430 (1640), 325 (sh), 280 (262010), 245 (sh) nm.

***Caution*:** During handling of the perchlorate salts of metal complexes with organic ligands care should be taken because of the possibility of explosions.

Data Collection and Structure Refinement: A crystal of suitable size was selected after careful examination under an optical microscope. Intensity data for the crystal were collected using Mo-K_α (λ = 0.71073 Å) radiation with a Siemens three circle diffractometer attached with a CCD area at 293 K. The crystallographic data are collected in Tables 5 and 6. The SMART[55] program was used for collecting frames of data, indexing the reflections, and determination of lattice parameters; the SAINT[55] program was used for the integration of the intensity of reflections and scaling; the SADABS[56] program was used for absorption corrections. The structure was solved by the Patterson method using the SHELXS-97 program[57] and refined by the full-matrix least-squares method on F^2 using the SHELXL-97 program.[57] The non-hydrogens were refined anisotropically. The nitrogen atom of the uncoordinated acetonitrile molecule is disordered and the site occupancies were given as 0.4 and 0.6. The hydrogen atoms were geometrically fixed at calculated positions. The molecular structure was drawn using the POV-ray.[58]

Table 5. Selected bond lengths [Å] and angles [°] for $[Ru(ntb)Cl_2]Cl·CH_3CN·2H_2O$ (**1**).[a]

Ru(1)–N(6)	2.041(5)	N(6)–Ru(1)–N(4)	162.09(17)
Ru(1)–N(4)	2.047(5)	N(6)–Ru(1)–N(2)	88.25(18)
Ru(1)–N(2)	2.069(4)	N(4)–Ru(1)–N(2)	87.36(17)
Ru(1)–N(1)	2.119(4)	N(6)–Ru(1)–N(1)	81.01(17)
Ru(1)–Cl(1)	2.3757(15)	N(4)–Ru(1)–N(1)	81.23(17)
Ru(1)–Cl(2)	2.3949(14)	N(2)–Ru(1)–N(1)	83.06(17)
		N(6)–Ru(1)–Cl(1)	90.70(14)
		N(4)–Ru(1)–Cl(1)	91.86(13)
		N(2)–Ru(1)–Cl(1)	174.00(13)
		N(1)–Ru(1)–Cl(1)	90.94(12)
		N(6)–Ru(1)–Cl(2)	98.76(13)
		N(4)–Ru(1)–Cl(2)	99.02(13)
		N(2)–Ru(1)–Cl(2)	97.36(13)
		N(1)–Ru(1)–Cl(2)	179.52(12)
		Cl(1)–Ru(1)–Cl(2)	88.64(5)

[a] Standard deviations in parenthesis.

Table 6. Selected crystallographic data for $[Ru(ntb)Cl_2]Cl·CH_3CN·2H_2O$ (**1**).

Empirical formula	$C_{26}H_{28}Cl_3N_8O_2Ru$
M_r [g mol^{-1}]	691.98
Crystal system	triclinic
Space group	$P\bar{1}$
a [Å]	9.9702(6)
b [Å]	11.1762(6)
c [Å]	14.2826(8)
α [°]	84.8837(13)
β [°]	73.9297(11)
γ [°]	74.2851(11)
V [Å]	1471.97(14)
Z	2
ρ_{calcd} [g cm^{-3}]	1.561
λ(Mo-K_α) [Å]	0.71073
T [K]	293(2)
Number of reflections collected	6197 (R_{int} = 0.0478)
Unique reflections with $I > 2.00\sigma(I)$	4125
Goodness-of-fit on F^2	0.982
R_1[a]	0.0411
wR_2[a]	0.0890

[a] $R_1 = \Sigma||F_o| - |F_c|| / \Sigma|F_o|$; $wR_2 = \{\Sigma[w[(F_o^2 - F_c^2)^2]/\Sigma[w(F_o^2)^2]\}^{1/2}$.

CCDC-652838 contains the supplementary crystallographic data for this paper. These data can be obtained free of charge from The Cambridge Crystallographic Data Centre via www.ccdc.cam.ac.uk/data_request/cif.

Catalytic Oxidations: The oxidation of substrates was carried out in methanol as the solvent at room temperature under both aerobic and anaerobic conditions. Catalytic amounts of the complex (1.0×10^{-4} M) were dissolved in 5 mL of CH_3OH and 1 M of alkanes/alkenes, and the oxidant *tert*-butyl hydroperoxide (TBHP)/*m*-chloroperbenzoic acid (*m*-CPBA)/hydrogen peroxide (H_2O_2) (1.0×10^{-1} M) was then added to it. After stirring for 12 h an aliquot (1.0 mL) was taken from the reaction mixture, filtered through a silica column, and the silica washed with ethyl ether. The sample solution was concentrated to 1 mL by passing nitrogen gas over it and 1 mL of bromobenzene in ethyl ether (0.080 M) was added as an internal standard. The organic products in the mixture were identified by a Perkin–Elmer Clarus 500 GC–MS and quantitatively analyzed by a HP 6890 series GC equipped with a HP-5

capillary column (30 m × 0.32 mm × 2.5 μm). The oxidation of cyclohexane and cyclohexene was carried out under an atmosphere of nitrogen also using the same procedure. Control reactions without catalysts were carried out under identical conditions.

Acknowledgments

We thank the Department of Science and Technology, India (Grant No. SP/S1/F-10/92 and SP/S1/F-20/2001) for the financial support. M. M. and R. M. thank the Council of Scientific and Industrial research, New Delhi for a Senior Research Fellowship. The authors thank the Regional Sophisticated Instrumentation Centre, Indian Institute of Technology, Chennai, India for the EPR facility. We thank Professor C. N. R. Rao, F. R. S. and Dr. G. U. Kulkarni Jawaharlal Nehru Centre for Advanced Scientific Research, Bangalore, India for providing the X-ray diffraction facility. We thank Professor A. Chakravorty, Indian Association for the Cultivation of Science, Kolkata, India for providing the software for the calculation of EPR distortion parameters. We thank one of the referees for his/her valuable comments on the catalytic mechanisms.

[1] R. H. Holm, *Chem. Rev.* **1987**, *87*, 1401; D. Ostovic, T. C. Bruice, *Acc. Chem. Res.* **1992**, *25*, 314; B. Meunier, *Chem. Rev.* **1992**, *92*, 1411; J. M. Mayer, *Acc. Chem. Res.* **1998**, *31*, 441.
[2] *Cytochrome P-450: Structure, Mechanism and Biochemistry*, 2nd ed. (Ed. P. R. Ortiz de Montellano), Plenum Press, New York, **1995**.
[3] Y. Dong, H. Fujii, M. P. Hendrich, R. A. Leising, G. Pan, C. R. Randall, E. C. Wilkinson, Y. Zang, L. Que Jr., B. G. Fox, K. Kauffman, E. Münck, *J. Am. Chem. Soc.* **1995**, *117*, 2778; C. Kim, Y. Dong, L. Que Jr., *J. Am. Chem. Soc.* **1997**, *119*, 3635; Y. Dong, Y. Zang, L. Shu, E. C. Wilkinson, L. Que Jr., *J. Am. Chem. Soc.* **1997**, *119*, 12683; H.-F. Hsu, Y. Dong, L. Shu, V. G. Young Jr., L. Que Jr., *J. Am. Chem. Soc.* **1999**, *121*, 5230; J. Kim, Y. Dong, E. Larka, L. Que Jr., *Inorg. Chem.* **1996**, *35*, 2369.
[4] K. Chen, M. Costas, J. Kim, A. K. Tipton, L. Que Jr., *J. Am. Chem. Soc.* **2002**, *124*, 3026; M. Costas, L. Que Jr., *Angew. Chem. Int. Ed.* **2002**, *41*, 2179; M. Fujita, M. Costas, L. Que Jr., *J. Am. Chem. Soc.* **2003**, *125*, 9912; M. C. White, A. G. Doyle, E. N. Jacobsen, *J. Am. Chem. Soc.* **2001**, *123*, 7194; J. Y. Ryu, J. Kim, M. Costas, K. Chen, W. Nam, L. Que Jr., *Chem. Commun.* **2002**, 1288; T. Kojima, R. A. Leising, S. Yan, L. Que Jr., *J. Am. Chem. Soc.* **1993**, *115*, 11328; M. Kodera, M. Itoh, K. Kano, T. Funabiki, M. Reglier, *Angew. Chem. Int. Ed.* **2005**, *44*, 7104; G. Dubois, A. Murphy, T. D. P. Stack, *Org. Lett.* **2003**, *5*, 2469.
[5] C.-M. Che, V. W.-W. Yam, *Adv. Inorg. Chem.* **1992**, *39*, 233.
[6] W. P. Griffith, *Chem. Soc. Rev.* **1992**, *21*, 179.
[7] T. Naota, H. Takaya, S.-I. Murahashi, *Chem. Rev.* **1998**, *98*, 2599.
[8] W.-H. Fung, W.-Y. Yu, C.-M. Che, *J. Org. Chem.* **1998**, *63*, 7715.
[9] J. T. Groves, R. Quinn, *J. Am. Chem. Soc.* **1985**, *107*, 5790.
[10] T.-S. Lai, R. Zhang, K.-K. Cheung, H.-L. Kwong, C.-M. Che, *Chem. Commun.* **1998**, 1583.
[11] R. Neumann, M. Dahan, *J. Am. Chem. Soc.* **1998**, *120*, 11969.
[12] T. Kojima, T. Amano, Y. Ishii, M. Ohba, Y. Okaue, Y. Matsuda, *Inorg. Chem.* **1998**, *37*, 4076.
[13] T. Kojima, R. A. Leising, S. Yan, L. Que Jr., *J. Am. Chem. Soc.* **1993**, *115*, 11328.
[14] T. Kojima, *Chem. Lett.* **1996**, 121.
[15] T. Kojima, H. Matsuo, Y. Matsuda, *Inorg. Chim. Acta* **2000**, *300–302*, 661–667.
[16] K. Jitsukawa, Y. Oka, S. Yamaguchi, H. Masuda, *Inorg. Chem.* **2004**, *43*, 8119.
[17] M. Yamaguchi, H. Kousaka, S. Izawa, Y. Ichii, T. Kumano, D. Masui, T. Yamagishi, *Inorg. Chem.* **2006**, *45*, 8342.
[18] C.-Y. Su, B.-S. Kang, T.-B. Wen, Y.-X. Tong, X.-P. Yang, C. Zhang, H.-Q. Liu, J. Sun, *Polyhedron* **1999**, *18*, 1577.
[19] R. Viswanathan, M. Palaniandavar, T. Balasubramanian, P. T. Muthiah, *Inorg. Chem.* **1998**, *37*, 2943.
[20] B. Kwak, K. W. Cho, M. Pyo, M. S. Lah, *Inorg. Chim. Acta* **1999**, *290*, 21.
[21] J.-U. Rohde, J.-H. In, M. H. Lim, W. W. Brennessel, M. R. Bukowski, A. Stubna, E. Munck, W. Nam, L. Que Jr., *Science* **2003**, *299*, 1037; A. Liu, R. Y. N. Ho, L. Que Jr., M. J. Ryle, B. S. Phinney, R. P. Hausinger, *J. Am. Chem. Soc.* **2001**, *123*, 5126.
[22] J. Emerson, M. J. Clarke, W.-L. Ying, D. R. Sanadi, *J. Am. Chem. Soc.* **1993**, *115*, 11799.
[23] A. R. Oki, P. R. Bommarreddy, H. Zhang, N. Hosmane, *Inorg. Chim. Acta* **1995**, *231*, 109.
[24] K. Sakai, Y. Yamada, T. Tsubomura, *Inorg. Chem.* **1996**, *35*, 3136.
[25] R. M. Buchanan, R. J. O'Brien, J.-M. Latour, *Inorg. Chim. Acta* **1993**, *214*, 33.
[26] S. Wang, Q. Luo, X. Wang, L. Wang, K. Yu, *J. Chem. Soc., Dalton Trans.* **1995**, 2045.
[27] M. Scarpellini, J. C. Toledo Jr., A. Neves, J. Ellena, E. E. Castellano, D. W. Franco, *Inorg. Chim. Acta* **2004**, *357*, 707.
[28] L. Ion, D. Morales, J. Pérez, L. Riera, V. Riera, R. A. Kowenicki, M. McPartlin, *Chem. Commun.* **2006**, 91; S. Rau, L. Bottcher, S. Schebesta, M. Stollenz, H. Gorls, D. Walther, *Eur. J. Inorg. Chem.* **2002**, *11*, 2800; S. Rau, M. Ruben, T. Buttner, C. Temme, S. Dautz, H. Gorls, M. Rudolph, D. Walther, A. Brodkorb, M. Duati, C. O'Connor, J. G. Vos, *J. Chem. Soc., Dalton Trans.* **2000**, 3649.
[29] C.-M. Che, S.-S. Kwong, C.-K. Poon, T.-F. Lai, T. C. W. Mak, *Inorg. Chem.* **1985**, *24*, 1359.
[30] E. Verdonck, L. G. Vanquickenborne, *Inorg. Chem.* **1974**, *13*, 762; J. A. Broomhead, L. A. P. Kane-Maquire, *J. Chem. Soc. A* **1967**, 546.
[31] G. K. Lahiri, S. Bhattacharya, S. Goswami, A. Chakravorty, *J. Chem. Soc., Dalton Trans.* **1990**, 561.
[32] P. S. Rao, G. A. Thakur, G. K. Lahiri, *Indian J. Chem. Sect. A* **1996**, *35*, 946.
[33] A. Premanik, N. Bag, G. K. Lahiri, A. Chakravorty, *J. Chem. Soc., Dalton Trans.* **1990**, 3823.
[34] B. Bleaney, M. C. M. O'Brien, *Proc. Phys. Soc. London Sect. B* **1956**, *69*, 1216.
[35] J. S. Griffith, *The Theory of Transition Metal Ions*, Cambridge University Press, London, **1961**, p. 364.
[36] S. Bhattacharya, A. Chakravorty, *Proc. Indian Acad. Sci. Chem. Sci.* **1985**, *95*, 159.
[37] R. E. Desimone, *J. Am. Chem. Soc.* **1973**, *95*, 6238.
[38] N. J. Hill, *J. Chem. Soc. Faraday Trans.* **1972**, 427.
[39] C. J. Ballhausen, *Introduction to Ligand Field Theory*, McGraw-Hill, New York, 1962, p. 99.
[40] P. Munshi, R. Samanta, G. K. Lahiri, *J. Organomet. Chem.* **1999**, *586*, 176.
[41] K. Jitsukawa, Y. Oka, H. Einaga, H. Masuda, *Tetrahedron Lett.* **2001**, *42*, 3467.
[42] C.-M. Che, V. W.-W. Yam, *Adv. Inorg. Chem.* **1992**, *39*, 233; W. P. Griffith, *Chem. Soc. Rev.* **1992**, *21*, 179; T. Naota, H. Takaya, S.-I. Murahashi, *Chem. Rev.* **1998**, *98*, 2599; T. Kojima, H. Matsuo, Y. Matsuda, *Inorg. Chim. Acta* **2000**, *300–302*, 661; D. Chetterjee, A. Mitra, S. Mukherjee, *Polyhedron* **1999**, *18*, 2659; M. M. Taquikhan, D. Chetterjee, R. R. Merohant, P. Paul, S. H. R. Abdi, D. Srinivas, M. R. H. Siddqui, M. A. Moiz, M. M. Bhadbhade, K. Vekatasubramanian, *Inorg. Chem.* **1992**, *31*, 2711; A. S. Goldstein, R. S. Drago, *J. Chem. Soc., Chem. Commun.* **1991**, 21.
[43] C. Che, C. Ho, T. C. Lau, *J. Chem. Soc., Dalton Trans.* **1991**, 1259.
[44] G. A. Barf, R. A. Sheldon, *J. Mol. Catal. A* **1995**, *102*, 23.

[45] T. A. van den Berg, J. W. de Boer, W. R. Browne, G. Roelfes, B. L. Feringa, *Chem. Commun.* **2004**, 2550.
[46] L. K. Stultz, M. H. V. Huynh, R. A. Binstead, M. Curry, T. J. Meyer, *J. Am. Chem. Soc.* **2000**, *122*, 5984.
[47] C.-J. Liu, W.-Y. Yu, C.-M. Che, C.-H. Yeung, *J. Org. Chem.* **1999**, *64*, 7365; W.-H. Fung, W.-Y. Yu, C.-M. Che, *J. Org. Chem.* **1998**, *63*, 7715.
[48] W.-C. Cheng, W.-Y. Yu, C.-K. Li, C.-M. Che, *J. Org. Chem.* **1995**, *60*, 6840.
[49] F. R. Mayo, *Acc. Chem. Res.* **1968**, *1*, 193.
[50] A. S. Kanmani, S. Vancheesan, *J. Mol. Catal. A* **1997**, *125*, 127.
[51] L. K. Thompson, B. S. Ramaswamy, E. A. Seymour, *Can. J. Chem.* **1977**, *55*, 878.
[52] C.-Y. Su, B.-S. Kang, C.-X. Du, Q.-C. Yang, T. C. W. Mak, *Inorg. Chem.* **2000**, *39*, 4843.
[53] M. J. Root, E. Deutsch, *Inorg. Chem.* **1985**, *24*, 1464.
[54] V. D. Parker, in: *Electroanalytical Chemistry* (Ed.: A. J. Bard), Marcel Dekker, New York, **1986**, vol. 14, p. 18.
[55] Siemens Analytical X-ray Instruments Inc., **1995**, Madison, Wisconsin, USA.
[56] G. M. Sheldrick, *"SADABS User Guide"*, University of Göttingen, Germany, **1993**.
[57] G. M. Sheldrick, *SHELXS-97, Program for Crystal Structure Determination*, University of Göttingen, Germany, **1997**.
[58] L. J. Farrugia, "*POV-Ray - 3.5*", Glasgow University, Australia, **2003**.

Received: February 3, 2009
Published Online: June 22, 2009

